Atmos. Chem. Phys., 19, 649–661, 2019
https://doi.org/10.5194/acp-19-649-2019

Atmospheric Chemistry and Physics
Open Access
EGU

A potential source of atmospheric sulfate from O_2^--induced SO_2 oxidation by ozone

Narcisse Tchinda Tsona and Lin Du

Environment Research Institute, Shandong University, Binhai Road 72, 266237 Shandong, China

Correspondence: Lin Du (lindu@sdu.edu.cn)

Received: 19 October 2018 – Discussion started: 5 November 2018
Revised: 2 January 2019 – Accepted: 6 January 2019 – Published: 17 January 2019

Abstract. It was formerly demonstrated that O_2SOO^- forms at collisions rate in the gas phase as a result of SO_2 reaction with O_2^-. Here, we present a theoretical investigation of the chemical fate of O_2SOO^- by reaction with O_3 in the gas phase, based on ab initio calculations. Two main mechanisms were found for the title reaction, with fundamentally different products: (i) formation of a van der Waals complex followed by electron transfer and further decomposition to $O_2 + SO_2 + O_3^-$ and (ii) formation of a molecular complex from O_2 switching by O_3, followed by SO_2 oxidation to SO_3^- within the complex. Both reactions are exergonic, but separated by relatively low energy barriers. The products in the former mechanism would likely initiate other SO_2 oxidations as shown in previous studies, whereas the latter mechanism closes a path wherein SO_2 is oxidized to SO_3^-. The latter reaction is atmospherically relevant since it forms the SO_3^- ion, hereby closing the SO_2 oxidation path initiated by O_2^-. The main atmospheric fate of SO_3^- is nothing but sulfate formation. Exploration of the reactions kinetics indicates that the path of reaction (ii) is highly facilitated by humidity. For this path, we found an overall rate constant of 4.0×10^{-11} cm^3 molecule^{-1} s^{-1} at 298 K and 50 % relative humidity. The title reaction provides a new mechanism for sulfate formation from ion-induced SO_2 oxidation in the gas phase and highlights the importance of including such a mechanism in modeling sulfate-based aerosol formation rates.

1 Introduction

The chemistry of sulfur is highly important in the atmosphere. Through its oxidation products, sulfur participates in the formation of secondary atmospheric aerosols, clouds, and acid rain. Sulfur dioxide (SO_2), the most abundant sulfur-containing molecule in the atmosphere, is known to react both in the gas phase and in multiphase oxidation processes following different mechanisms to form sulfate as the final oxidation species. The main SO_2 oxidizers in the gas phase include the hydroxyl radical (OH) (Seinfeld and Pandis, 2016), stabilized Criegee intermediates (Welz et al., 2012; Mauldin III et al., 2012; Vereecken et al., 2012), and atmospheric ions (Fehsenfeld and Ferguson, 1974; Enghoff et al., 2012; Tsona et al., 2015). The main routes for SO_2 heterogeneous/multiphase oxidation include reactions with mineral dust (Harris et al., 2013), O_3 and H_2O_2 in cloud droplets (Caffrey et al., 2001; Hoyle et al., 2016; Harris et al., 2012; Hegg et al., 1996), and NO_2 and O_2 in aerosol water and on $CaCO_3$ particles (Cheng et al., 2016; Wang et al., 2016; Zhang et al., 2018; Yu et al., 2018; Zhao et al., 2018). In the gas phase, the SO_2 oxidation by OH and Criegee intermediates leads to SO_3 that ultimately forms H_2SO_4 (Larson et al., 2000), whereas reactions with ions are generally more complex. In the aqueous phase, SO_4^{2-} is formed as the terminal oxidation species. Sulfate is known to be the main driving species in atmospheric aerosols formation and its formation is critical in the determination of aerosol formation rates (Nieminen et al., 2009; Sipilä et al., 2010; Kuang et al., 2008; Kulmala et al., 2000). The role of ions in this formation has been well established (Yu, 2006; Yu and Turco, 2000, 2001; Enghoff and Svensmark, 2008; Kirkby et al., 2011; Wagner et al., 2017; Yan et al., 2018), although relatively minor compared to the mechanism involving neutral particles exclusively (Eisele et al., 2006; Manninen et al., 2010; Kirkby et al., 2011; Hirsikko et al., 2011; Wagner et al., 2017).

The immediate products of SO_2 oxidation by ions are mostly sulfur oxide ion intermediates (Fehsenfeld and Ferguson, 1974; Möhler et al., 1992; Bork et al., 2012; Tsona et al., 2014) that are susceptible to the triggering of new reactions or recombination with oppositely charged counterparts to form neutral species. Some of these ions, namely SO_3^-, SO_4^-, and SO_5^-, were detected at relatively high concentrations in the ambient atmosphere (Ehn et al., 2010) and in chamber experiments of SO_2 ionic oxidation studies (Nagato et al., 2005; Hvelplund et al., 2013; Kirkby et al., 2011, 2016). The chemical fate of most sulfur oxides anions is relatively known. Bork et al. (2012) showed that SO_3^- can form SO_3, the precursor for H_2SO_4, through electron transfer to ozone (O_3) (Bork et al., 2012). SO_3^- can equally react with O_2 to form SO_5^-, whose atmospheric outcome by reaction with O_3 is H_2SO_4 formation (Bork et al., 2013). It was also speculated from chamber studies that SO_5^- could form and stabilize clusters with sulfuric acid in the gas phase (Kirkby et al., 2011). Reliable predictions of the outcomes of these ions require an exact knowledge of their chemical structures since interactions between molecules or ions depend both on their physical and chemical properties. A previous study demonstrated that two forms of SO_4^- separated by a high energy barrier may exist in the atmosphere (Tsona et al., 2014): the sulfate radical ion henceforth indicated as SO_4^-, and the peroxy form, O_2SOO^-, in which the O_2S–OO^- bond nature is more dative than covalent. Formerly, the two isomers were often misleadingly attributed exclusively to the sulfate radical ion, the most stable form of SO_4^-. However, their reactive properties greatly differ (Fehsenfeld and Ferguson, 1974).

The formation mechanisms of SO_4^- in the gas phase have been largely unknown but, recent studies showed that this ion can be formed by SO_5^- reaction with O_3 (Bork et al., 2013) and in a O_2SOO^- isomerization process catalyzed by NO (Tsona et al., 2018). SO_4^- can also be produced during the chemical transformation of organic compounds, triggered by sulfate salts (Noziere et al., 2010), whereas O_2SOO^- is formed at collision rates upon SO_2 reaction with O_2^- (Fahey et al., 1982; Tsona et al., 2014).

The sulfate radical ion is believed to react with unsaturated compounds to form organosulfates, a major component of secondary organic aerosol (Surratt et al., 2007, 2008; Schindelka et al., 2013). Using first-principle calculations, SO_4^- was shown to act as a catalyst in SO_2 oxidation to SO_3 by O_3 in the gas phase and, hence, plays a role in atmospheric aerosol formation (Tsona et al., 2015, 2016). The chemistry of O_2SOO^- is largely unknown, although potentially important for sulfur chemistry and atmospheric aerosol formation. Fehsenfeld and Ferguson found that O_2SOO^- can be decomposed by NO_2 into NO_3^- and SO_3 (Fehsenfeld and Ferguson, 1974) and a recent study showed that in the presence of nitrogen oxides ($NO_x = NO_2 + NO$), O_2SOO^- can be converted into sulfate (Tsona et al., 2018). In mildly polluted environments, the concentration of O_3 can be a few orders of magnitude higher than that of NO_x and the chemical fate of O_2SOO^- would then also greatly depend on collisions with O_3. In such environments, O_2SOO^- could experience much more collisions with O_3 than with NO_x.

Hereby, we investigate the reaction between $O_2SOO^- \cdots (H_2O)_{0-1}$ and O_3 using ab initio calculations. By determining the reactions' thermodynamics and kinetics, we examine the possible pathways for the reaction and propose the most probable outcome of $O_2SOO^- \cdots (H_2O)_{0-1}$ based on the O_3 reaction. Implications of the most relevant pathways for aerosol formation are discussed.

2 Methods

2.1 Geometry optimizations and thermochemical and charge analysis

As the substrate in this study is a radical anion, all stationary points in the energy surface were optimized using density functional theory (DFT) based on the UM06-2X density functional (Zhao and Truhlar, 2008) and the aug-cc-pVTZ basis set (Dunning Jr. et al., 2001), setting the charge to -1 and the spin multiplicity to 2. The use of UM06-2X implies the use of unrestricted wave functions to describe the quantum state of the system. Spin contamination often arises from unrestricted DFT calculations and it is not guaranteed that the electronic states from these calculations are eigenstates of the $\hat{S}^2$ operator. The spin contamination was then evaluated for all electronic states as $\Delta S = \langle \hat{S}^2 \rangle - \langle \hat{S}^2 \rangle_{\text{ideal}}$, where $\langle \hat{S}^2 \rangle$ is the actual value of the expectation value of the $\hat{S}^2$ operator from DFT calculations and $\langle \hat{S}^2 \rangle_{\text{ideal}}$ is the ideal expectation value. For systems explored in this study, $\langle \hat{S}^2 \rangle_{\text{ideal}} = 0.75$.

The UM06-2X functional has successfully proven to be adequate for reactions involving transition state (TS) configurations (Elm et al., 2012, 2013a, b). Harmonic vibrational frequency analyses on the optimized structures were performed (at 298 K and 1 atm) using the UM06-2X/aug-cc-pVTZ method under the harmonic oscillator–rigid rotor approximation. These calculations ensured that the stationary points obtained were minima or TS and, also, provided the thermal contributions to the Gibbs free energy and the enthalpy.

Transition-state structures were initially located by scanning the reactants configurations. The best TS guesses from the scans were then refined using the synchronous transit quasi-Newton method (Peng et al., 1996), and the final TS structures underwent internal reaction coordinate calculations (Fukui, 1981) to ensure they connected the reactants to desired products.

The electronic energies of the UM06-2X/aug-cc-pVTZ optimized geometries were corrected using the UCCSD(T) method (Purvis and Bartlett, 1982) in conjunction with the aug-cc-pVTZ basis set. The Gibbs free

energies, G, of all relevant species were then calculated as

$$G = E_{\mathrm{UCCSD(T)}} + G_{\mathrm{therm}}, \quad (1)$$

where $E_{\mathrm{UCCSD(T)}}$ is the electronic energy calculated using the UCCSD(T)/aug-cc-pVTZ method and G_{therm} is the thermal contribution to the Gibbs free energy, calculated at the UM06-2X/aug-cc-pVTZ level of theory. All geometry optimizations, harmonic vibrational frequency analysis, and electronic energy correction calculations were carried out in the Gaussian 09 package (Frisch et al., 2013).

To analyze the distribution of the excess electronic charge over different species and fragments in the optimized systems, we used the atoms-in-molecules charge partitioning method presented by Bader (Bader, 1998). This is an intuitive way of dividing the molecules of a system into atoms, which are purely defined in terms of electronic charge density. The Bader charge partitioning assumes that the charge density between atoms of a molecular system reaches a minimum, which is an ideal place to separate atoms from each other. As input, this method requires electronic density and nuclear coordinates from electronic structure calculations. We used the approach implemented in the algorithm developed by Henkelman and co-workers, which has been shown to work well both for charged and water-containing systems (Tang et al., 2009; Bork et al., 2011; Henkelman et al., 2006).

2.2 Reactions kinetics

Regardless of the presence of water, the reaction between O_2SOO^- and O_3 begins by forming different van der Waals pre-reactive intermediates, depending on the orientation of the reactants at impact. The pre-reactive intermediate could either decompose to different species or react further through a transition state configuration to form new products:

$$O_2SOO^- + O_3 \leftrightarrow \text{ pre-reactive intermediate } \rightarrow \text{ products.} \quad (R1)$$

The traditional approach to determine the rate constant of Reaction (R1) relies on the steady-state approximation and leads to the following equation:

$$k = k_{\mathrm{coll}} \frac{k_{\mathrm{reac}}}{k_{\mathrm{reac}} + k_{\mathrm{evap}}}, \quad (2)$$

where k_{coll} is the collision frequency for O_2SOO^-–O_3 collisions, k_{evap} is the rate constant for the evaporation of the pre-reactive intermediate back to initial reactants, and k_{reac} is the unimolecular rate constant for the reaction of the pre-reactive intermediate to the products. Moreover, assuming that $k_{\mathrm{evap}} \gg k_{\mathrm{reac}}$, the rate constant of Reaction (R1) becomes $k = K_{\mathrm{eq}} k_{\mathrm{reac}}$ over a range of temperatures, with K_{eq} being the equilibrium constant of formation of the pre-reactive intermediate from the reactants. This consideration is, however, not valid for reactions with a submerged barrier, since the pre-reactive intermediate seldom thermally equilibrates. For such reactions, a two-transition-state theory has been introduced, treating two distinct transition state bottlenecks that define the net reactive flux (Klippenstein et al., 1988; Georgievskii and Klippenstein, 2005; Greenwald et al., 2005). The first bottleneck, the "outer" transition state, occurs in the association of the initial reactants to form the pre-reactive intermediate, whereas the second bottleneck, the "inner" transition state, occurs in the transformation of the pre-reactive intermediate to the products. Based on this theory, the overall rate constant (k) for a reaction channel is expressed in terms of the outer (k_{out}) and inner (k_{in}) rate constants as

$$\frac{1}{k} = \frac{1}{k_{\mathrm{out}}} + \frac{1}{k_{\mathrm{in}}}. \quad (3)$$

The outer transition state is treated by the long-range transition state theory approach (Georgievskii and Klippenstein, 2005), while the inner transition state is resolved by the transition state theory. It was shown that for interactions between ions and neutral molecules, due to their long-range attraction, the collision cross section is larger than would be measured from the physical dimensions of the colliding species (Kupiainen-Määttä et al., 2013). To account for this phenomenon, the outer rate constant was determined from the ion–dipole parametrization of Su and Chesnavich, who performed trajectory simulations of collisions between a point charge and a rigidly rotating molecule (Su and Chesnavich, 1982). This parametrization is equivalent to a Langevin capture rate constant (k_{L}) scaled by a temperature-dependent term and was found to provide good agreement with experiments (Kupiainen-Määttä et al., 2013). It is given as

$$k_{\mathrm{out}} = k_{\mathrm{L}} \times \left(\frac{(x + 0.5090)^2}{10.526} + 0.9754 \right), \quad (4)$$

where $k_{\mathrm{L}} = q\mu^{-1/2}(\pi\alpha/\varepsilon_0)^{1/2}$, $x = \mu_{\mathrm{D}}/(8\pi\varepsilon_0\alpha k_{\mathrm{B}}T)^{1/2}$, q is the charge of the ion, μ is the reduced mass of the colliding species, ε_0 is the vacuum permittivity, α and μ_{D} are the polarizability and dipole moment of the neutral molecule (ozone), k_{B} is Boltzmann's constant, and T is the absolute temperature. The inner rate constant can be written as

$$k_{\mathrm{in}} = \frac{k_{\mathrm{B}}T}{hc^0} \times \exp\left(-\frac{\Delta G^{\ddagger}}{RT} \right), \quad (5)$$

where $\Delta G^{\ddagger}$ is the Gibbs free energy barrier separating the pre-reactive intermediate and the products, h is the Planck's constant, R is the molar gas constant, and c^0 is the standard gas-phase concentration. The constants and variables in Eqs. (4) and (5) are given in the centimeter-gram-second (CGS) system of units and International System (SI) units, respectively. Details on these units are given in the Supplement.

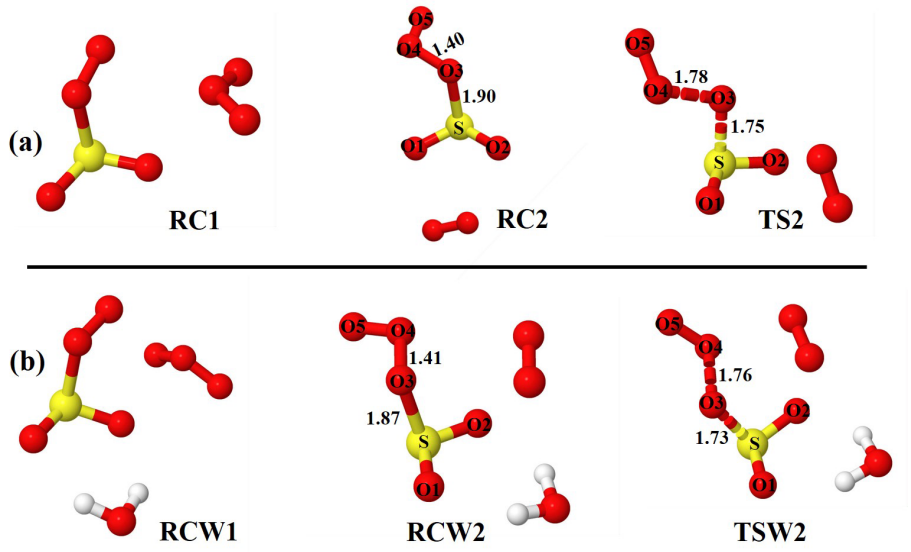

Figure 1. Optimized structures of the most stable intermediates in the $O_2SOO^- + O_3$ reaction **(a)** in the absence and **(b)** in the presence of a single water molecule. Optimizations were performed at the UM06-2X/aug-cc-pVTZ level of theory. Lengths (in Å) of some descriptive bonds are indicated. The color coding is yellow for sulfur, red for oxygen, and white for hydrogen.

3 Results and discussion

Starting with optimized structures of $O_2SOO^- \cdots (H_2O)_{0-1}$ and O_3 shown in Fig. S1 in the Supplement, a series of geometry optimizations was performed on the $O_2SOO^- \cdots (H_2O)_{0-1} + O_3$ system, taking into account different spatial orientations of the reactants at impact. These optimizations led to two main chemical processes, depending on the initial orientation of the reactants, with potentially different outcomes. The first process is the formation of a van der Waals complex followed by its direct decomposition to other species. The second process is the low-lying formation of a molecular complex in which the SO_2 entity of $O_2SOO^- \cdots (H_2O)_{0-1}$ is oxidized to SO_3^-.

3.1 Cluster formation and decomposition of $O_2SOO^- \cdots (H_2O)_{0-1}$

As O_3 approaches $O_2SOO^- \cdots (H_2O)_{0-1}$ towards the oxygen atoms of the peroxy fragment or the oxygen atom of the SO_2 moiety, the immediate outcome of $O_2SOO^- \cdots (H_2O)_{0-1}$ and O_3 collisions is the formation of the van der Waals $O_3 \cdots O_2SOO^- \cdots (H_2O)_{0-1}$ complex in which O_3 interacts with O_2SOO^-. Among the different stable configurations found upon optimization, we solely report the most stable one with respect to the Gibbs free energy, which is henceforth denoted RC1 and RCW1 for the unhydrated and monohydrated reactions, respectively, shown in Fig. 1. Exploration of the RC1 and RCW1 structures reveals that $O_2SOO^- \cdots (H_2O)_{0-1}$ basically keeps its configuration upon clustering with O_3. The spin contaminations for RC1 and RCW1 are negligible, being 0.0086 and 0.0081, respectively. The electronic energies of formation of RC1 and RCW1 are -5.1 and -4.6 kcal mol^{-1}, respectively. Despite the fact that these complexes may form at 0 K, the Gibbs free energies of their formation under atmospheric pressure and 298 K (4.5 and 4.7 kcal mol^{-1}, respectively) indicate that their formation is endergonic under atmospherically relevant conditions. These Gibbs free energy values indicate that, if formed, these complexes would not live long and will rather decompose either to initial reactants or to different species. Hence, the Gibbs free energies of formation of RC1 and RCW1 define the lowest states at which O_2SOO^- can interact with O_3 to allow electron transfer and O_2S–OO decomposition, and thus represent the energy barrier towards $O_2 + SO_2 + O_3^-$ formation. Inspecting the vibrational modes of RC1 and RCW1, two vibrations are found that would clearly lead to the dissociation of O_2SOO^- within the complex. The analysis of the charge distribution over $O_3 \cdots O_2SOO^- \cdots (H_2O)_{0-1}$ shows that the extra electron initially located on O_2SOO in the reactants has migrated to the O_3 molecule in the van der Waals product complex, as can be observed in Fig. S2. This is as expected, given the high electronegativity of O_3 relative to that of O_2 and SO_2 (Rothe et al., 1975). The charge distribution over the different atoms of the optimized complex is weakly affected by the presence of water, as previously demonstrated by Bork and co-workers (Bork et al., 2011).

The most likely fates of RC1 and RCW1 are, therefore, decomposition into O_2, SO_2, and O_3^- as follows:

$$O_2SOO^- \cdots (H_2O)_{0-1} + O_3 \leftrightarrow O_3 \cdots O_2SOO^- \cdots (H_2O)_{0-1} \rightarrow O_2 + SO_2 + O_3^- + (H_2O)_{0-1}. \quad \text{(R2)}$$

Table 1. Electronic energies (ΔE), enthalpies ($\Delta H_{298\,K}$), and Gibbs free energies ($\Delta G_{298\,K}$) of the different states in the $O_2SOO^- + O_3$ reaction both in the absence and in the presence of water, calculated relative to the energy of initial reactants at the UCCSD(T)/aug-cc-pVTZ//UM06-2X/aug-cc-pVTZ level of theory.

Species	ΔE	$\Delta H_{298\,K}$	$\Delta G_{298\,K}$
Unhydrated reaction			
$O_2SOO^- + O_3$	0	0	0
$RC1 = O_3 \cdots O_2SOO^-$	−5.1	−3.9	4.5
$RC2 = O_2 \cdots O_2S\text{–}O_3^-$	−21.9	−21.0	−14.7
TS2	−11.6	−11.9	−4.6
$SO_3^- + 2O_2$	−35.8	−36.4	−45.3
$O_2 + SO_2 + O_3^-$	−1.7	−3.2	−13.6
Monohydrated reaction			
$O_2SOO^- \cdots H_2O + O_3$	0	0	0
$RCW1 = O_3 \cdots O_2SOO^- \cdots H_2O$	−4.6	−3.4	4.7
$RCW2 = O_2 \cdots O_2S\text{–}O_3^- \cdots H_2O$	−21.9	−20.9	−12.4
TSW2	−25.3	−25.4	−16.4
$SO_3^- \cdots H_2O + 2O_2$	−36.7	−37.4	−46.6
$O_2 + SO_2 + O_3^- + H_2O$	10.3	7.1	−12.1

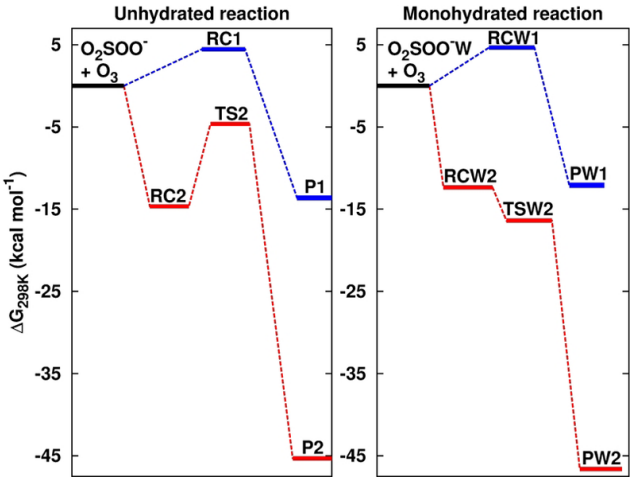

Figure 2. Formation Gibbs free energies of the most stable intermediate species in the $O_2SOO^- + O_3$ reaction in the absence and in the presence of water. "W" is the shorthand notation for water. RC1, RC2, TS2, RCW1, RCW2, and TSW2 structures are shown in Fig. 1. $P1 = O_2 + SO_2 + O_3^-$, $P2 = SO_3^- + 2O_2$, $PW1 = O_2 + SO_2 + O_3^- + H_2O$, and $PW2 = SO_3^- \cdots H_2O + 2O_2$. Calculations were performed at the UCCSD(T)/aug-cc-pVTZ//UM06-2X/aug-cc-pVTZ level of theory.

The numerical values of the formation energies of all intermediate species in Reaction (R2) are given in Table 1, and the energy surfaces are plotted in Fig. 2. RC1 and RCW1 decompositions are highly exergonic at 298 K, occurring with −18.1 and −16.7 kcal mol^{-1} Gibbs free energy changes, respectively. These processes are, therefore, likely to occur in the atmosphere upon formation of $O_3 \cdots O_2SOO^- \cdots (H_2O)_{0-1}$.

The limiting step in Reaction (R2) is the formation of RC1 and RCW1, whose formation energies indicated above can then be considered as the only barrier to the formation of $O_2 + SO_2 + O_3^-$. This leads to overall rate constants (according to Eq. 5) of 1.4×10^{-10} and 9.9×10^{-11} cm^3 molecule^{-1} s^{-1} at 298 K for the unhydrated and monohydrated reactions, respectively. Both reactions are, in principle, collision-limited and the effect of hydration on the kinetics is found to be negligible. The atmospheric relevance of Reaction (R2) has been determined already (Bork et al., 2012, 2013; Enghoff et al., 2012).

3.2 $O_2SOO^- \cdots (H_2O)_{0-1}$ reaction with O_3

When O_3 approaches $O_2SOO^- \cdots (H_2O)_{0-1}$ from the sulfur atom side, the formation of a more stable cluster than found above prevails. The incoming O_3 molecule strongly interacts with $O_2SOO^- \cdots (H_2O)_{0-1}$ by forming a coordination bond with the sulfur atom and hereby inducing the ejection of the O_2 molecule that remains in interaction with the remainder of the system. This process leads to the formation of the $O_2 \cdots O_2S\text{–}O_3^- \cdots (H_2O)_{0-1}$ complex which further transforms, through an intramolecular SO_2 oxidation, into $SO_3^- \cdots (H_2O)_{0-1} + 2O_2$ according to the following equation:

$$O_2SOO^- \cdots (H_2O)_{0-1} + O_3 \leftrightarrow O_2 \cdots O_2S - O_3^- \cdots (H_2O)_{0-1} \rightarrow SO_3^- \cdots (H_2O)_{0-1} + 2O_2. \quad \text{(R3)}$$

The configurations of the most stable intermediate structures in Reaction (R3) are given in Fig. 1. The charge analysis on this system indicates that the electronic charge on the pre-reactive complex is essentially on two oxygen atoms of the O_3 moiety that is coordinated to SO_2 as can be seen in Fig. 3a. The net charge on these two oxygen atoms is 1.04e, whereas the net charge on the free O_2 molecule is 0.01e. The latter value shows that the O_2 molecule formed in the pre-reactive complex has no unpaired electrons, and hence is a singlet. Although the charge is still on the O_3 moiety in the transition state configuration, it is mostly located on the oxygen atom bound to sulfur (Fig. 3b). The net charge on the two outer oxygen atoms of the O_3 moiety in the transition state has substantially decreased to 0.30e, while the charge on the free O_2 molecule has slightly increased to 0.04e. The strong decrease in the charge of the two outer oxygen atoms of O_3 from the pre-reactive complex to the transition state suggests that the O_2 molecule to form in the product will likely be a singlet. In the products (Fig. 3c), the old free O_2 molecule has a net charge of 1.99e, whereas the charge on the newly formed O_2 is 0.06e. The 1.99e charge on the old free O_2 molecule indicates the presence of unpaired electrons in its configuration, meaning that the singlet O_2 has been transformed into a triplet. This clearly shows that a spin flip has

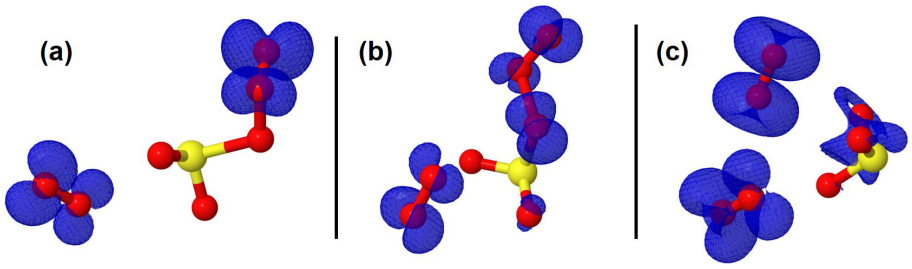

Figure 3. Representation of the spin density (in blue color) on intermediate structures in the $O_2SOO^- + O_3$ reaction. The spin density clearly indicates that the extra electron is progressively distributed over all the atoms from **(a)** the pre-reactive complex through **(b)** the transition state to **(c)** the product complex.

occurred in O_2 during further optimization of the products. The newly formed O_2 with 0.06*e* charge is obviously a singlet. This analysis shows for the unhydrated system that the singlet O_2 initially formed in the pre-reactive complex transforms into a triplet in the product state, while a new singlet O_2 is also formed. In the monohydrated system, the singlet O_2 initially formed in the pre-reactive complex remains as a singlet in the product state and a triplet O_2 is also released. Overall, the two forms of O_2 (singlet and triplet) are formed in the studied reaction, despite following different mechanisms. Although the water molecule in the monohydrated system does not retain any electric charge, it most likely stabilizes the initially formed singlet O_2 and prevents the spin flip.

Though the necessity to determine the electronic structure of the O_2 molecule in the singlet state ($^1\Delta_g$) has been demonstrated to be useful (Buttar and Hirst, 1994), obtaining a reliable electronic energy for $O_2(^1\Delta_g)$ is difficult (Drougas and Kosmas, 2005). An alternative approach to determine this energy is to add the experimental energy spacing (22.5 kcal mol^{-1}) between triplet and singlet states of O_2 to the computed electronic energy of the triplet O_2 (Schweitzer and Schmidt, 2003; Drougas and Kosmas, 2005). We used this approach to determine the energies of the products of Reaction (R3). The numerical values of the formation energies of all intermediate species in Reaction (R3) are thus given in Table 1 and the energy surfaces are plotted in Fig. 2. The most stable optimized structures of $O_2\cdots O_2S$–$O_3^-\cdots(H_2O)_{0-1}$ according to our calculations are denoted as RC2 and RCW2 for the unhydrated and monohydrated systems, respectively, and are shown in Fig. 1. Regardless of the presence of water, the $O_2\cdots O_2S$–O_3^- configuration results from O_2 being switched by O_3 in the O_2SOO^- molecular ion. In the optimized $O_2\cdots O_2S$–O_3^- structure, the O3 atom (labeled in Fig. 1) of O_3 points towards the S atom of O_2SOO^-, forming S–O3 bonds at distances of 1.90 and 1.87 Å in the absence and in the presence of water, respectively. These bonds are coordination bonds in nature since the S–O covalent bond is, e.g., 1.43 Å in SO_3 and 1.4 Å in H_2SO_4. The S–O3 coordination bond distances in RC2 and RCW2 are shorter by 0.04 and 0.03 Å than O_2S–OO^- bond distances in unhydrated and monohydrated O_2SOO^- forms. This indicates stronger interaction between O_3 and SO_2, and hence higher stability of $O_2\cdots O_2S$–O_3^- relative to O_2SOO^-.

The formations of RC2 and RCW2 are highly exergonic, with Gibbs free energy changes at 298 K of −14.7 and −12.4 kcal mol^{-1}, respectively. These values, with corresponding electronic energies and enthalpies, are shown in Table 1. These Gibbs free energy changes for the formation of RC2 and RCW2 are about 19 kcal mol^{-1} lower than those of RC1 and RCW1 at similar conditions, indicating the higher stability of RC2 and RCW2 and the highly favorable switching reaction at ambient conditions. SO_2 oxidation can readily occur within the $O_2\cdots O_2S$–$O_3^-\cdots(H_2O)_{0-1}$ cluster and lead to SO_3^- formation. In principle, to form the products of Reaction (R3), the O3 atom of the O_3 moiety in $O_2\cdots O_2S$–$O_3^-\cdots(H_2O)_{0-1}$ is transferred through transition state configurations, to SO_2 and forms SO_3^- followed by the ejection of the O_2 molecule. The transition states are denoted TS2 and TSW2 for the unhydrated and monohydrated systems, respectively, and their structures are presented in Fig. 1. While RC2 and RCW2 are formed with similar Gibbs free energies within 2 kcal mol^{-1} difference, the formation Gibbs free energies of their transition states at similar conditions greatly differ. TS2 is located at 10 kcal mol^{-1} Gibbs free energy above RC2, while TSW2 is located at −4 kcal mol^{-1} below RCW2. It is speculated that the low energy barrier in the monohydrated reaction is the result of a strong stabilization of the transition state due to hydration, with the S–O3 bonds in RCW2 and TSW2 shorter by ∼ 0.03 Å than in RC2 and TS2. Another reason for this substantial drop in the energy barrier is the difference in the electronic configurations of the two outer oxygen atoms of the O_3 moiety in the two transition states that form O_2 with different multiplicities in the products.

Based on the TS2 energy, the unimolecular decomposition of $O_2\cdots O_2S$–O_3^- at 298 K in the absence of water was found to occur at a rate constant of 3.1×10^5 s^{-1}, corresponding to an atmospheric lifetime of 3.3 µs. Both this short lifetime and the negative energy barrier of the monohydrated reaction indicate that $O_2\cdots O_2S$–O_3^- would not live long enough to experience collisions with other atmospheric oxidants. It

should be noted that few to no collisions with nitrogen can, however, be achieved. It follows that the most likely outcome of $O_2\cdots O_2S–O_3^-$ is decomposition to the products of Reaction (R3), which are formed with about $-46\,\mathrm{kcal\,mol^{-1}}$ overall Gibbs free energy at 298 K. The net reaction is an O_2^--initiated SO_2 oxidation to SO_3^- by O_3.

The spin contamination for electronic states in Reaction (R3) is quite significant, being 1.0122, 1.4666, and 2.0374 for the pre-reactive complex, transition state, and product, respectively, and is almost insensitive to the presence of water. The actual values of the expectation values of the $\hat{S}^2$ operator for all electronic states obtained from our calculations are given in the Supplement, along with their Cartesian coordinates. The high values of spin contamination likely reflect the formation of O_2 with different multiplicities within the system. As the charge analysis indicates, starting with singlet O_2 in the pre-reactive complexes of Reaction (R3), both singlet and triplet O_2 are formed in the final products.

The overall rate constants of Reaction (R3), determined at 298 K using Eq. (3), are 1.3×10^{-14} and $8.0\times10^{-10}\,\mathrm{cm^3\,molecule^{-1}\,s^{-1}}$ for the unhydrated and monohydrated reactions, respectively. The values of the different components (k_{out} and k_{in}) of these rate constants are listed in Table S1 of the Supplement. It is observed from Table S1 that the inner transition state provides the dominant bottleneck to the rate constant of the unhydrated reaction, whereas the outer transition state provides the dominant bottleneck to the rate constant of the monohydrated reaction.

The effective effect of water on the rate constant can be evaluated by taking into account the stability of $O_2SOO^-\cdots H_2O$ (which is formed at the entrance channel of the reaction in the presence of water before colliding with O_3) and the equilibrium vapor pressure of water. Starting from the definition of the reaction rate for the hydrated reaction,

$$J_{(\mathrm{R3w})} = k_{(\mathrm{R3w})}\times\left[O_2SOO^-\cdots H_2O\right]\times[O_3] \quad (6)$$

$$= k^{\mathrm{eff}}_{(\mathrm{R3w})}\times\left[O_2SOO^-\right]\times[O_3], \quad (7)$$

where $k_{(\mathrm{R3w})}$ is the overall rate constant for the hydrated reaction, determined using Eq. (3), and $k^{\mathrm{eff}}_{(\mathrm{R3w})}$ is the effective reaction rate constant calculated as $k^{\mathrm{eff}}_{(\mathrm{R3w})} = k_{(\mathrm{R3w})}\times K_{\mathrm{eq}}\times p_{H_2O}$. K_{eq} is the equilibrium constant for the $O_2SOO^- + H_2O \leftrightarrow O_2SOO^-\cdots H_2O$ reaction and p_{H_2O} the actual water vapor pressure. Details on the determination of K_{eq} and p_{H_2O} are given in the Supplement.

At 298 K and 50 % relative humidity, the effective rate constant of the monohydrated reaction is $1.7\times10^{-10}\,\mathrm{cm^3\,molecule^{-1}\,s^{-1}}$, 4 orders of magnitude higher than the rate constant of the unhydrated reaction. Therefore, water plays a catalytic role in the kinetics of Reaction (R3). The net rate constant of Reaction (R3) can be obtained by weighing the rate constants of the unhydrated and monohydrated reactions to corresponding equilibrium concentrations of $O_2\cdots O_2S–O_3^-$ hydrates. Using the law of mass action, we find that $O_2\cdots O_2S–O_3^-$ mostly exists as a dry species, constituting 77 % of the total population, whereas the monohydrated species forms 23 % of the total population. The net rate constant of Reaction (R3) is then determined to be $4.0\times10^{-11}\,\mathrm{cm^3\,molecule^{-1}\,s^{-1}}$ at 298 K.

Considering only the unhydrated process of Reaction (R3), the rate constant is 4–5 orders of magnitude lower than the rate constant obtained for the $SO_2 + O_3^- \rightarrow SO_3^- + O_2$ reaction (Fehsenfeld and Ferguson, 1974; Bork et al., 2012). Despite this difference, the oxidation process follows a similar mechanism to the one presented by Bork et al. for the $SO_2 + O_3^- \rightarrow SO_3^- + O_2$ reaction, consisting of the oxygen transfer from O_3 to SO_2 (Bork et al., 2012). The discrepancy between the two results is associated with the effect of the presence of the O–O fragment initially coordinated to SO_2 in the current study, which tends to stabilize the $O_2\cdots O_2S–O_3^-$ pre-reactive complex. The presence of the O–O fragment seemingly deactivates SO_2 for the upcoming O transfer from O_3 to form SO_3^-. However, this situation is rapidly reversed with the presence of water as the reaction becomes much faster, proceeding nearly at collision rate.

3.3 Further chemistry

In real atmospheric and ionized conditions, despite O_2 having lower electron affinity than O_3, it would likely ionize faster than O_3, owing to its much higher concentration. Considering, for example, chamber experiments, upon interaction of ionizing particles with the gas, electrons can transfer from one species to another and, e.g., O_2^- can form and rapidly hydrate within 1 ns (Svensmark et al., 2007; Fahey et al., 1982). Furthermore, Fahey et al. (1982) showed that the $O_2^-\cdots(H_2O)_{0-1}$ association reaction with SO_2 is faster than the electron transfer from $O_2^-\cdots(H_2O)_{0-1}$ to O_3 (Fahey et al., 1982). This means that in an ionized environment containing O_2, O_3, and SO_2, the formation of O_2SOO^- resulting from SO_2 and O_2^- association will happen faster than O_3^- formation. O_2SOO^- would react thereafter with O_3 and the following stepwise process could take place:

$$O_2^-\cdots(H_2O)_{0-1} + SO_2 \rightarrow O_2SOO^-\cdots(H_2O)_{0-1} \quad (\mathrm{R4a})$$

$$O_2SOO^-\cdots(H_2O)_{0-1} + O_3 \rightarrow O_2\cdots O_2S-O_3^- \cdots(H_2O)_{0-1} \quad (\mathrm{R4b})$$

$$O_2\cdots O_2S-O_3^-\cdots(H_2O)_{0-1} \rightarrow SO_3^-\cdots(H_2O)_{0-1} + 2O_2 \quad (\mathrm{R4c})$$

$$\mathrm{Net:}\ O_2^-\cdots(H_2O)_{0-1} + SO_2 + O_3 \rightarrow SO_3^- \cdots(H_2O)_{0-1} + 2O_2. \quad (\mathrm{R4})$$

The Gibbs free energy change of this net reaction at 298 K is about $-40\,\mathrm{kcal\,mol^{-1}}$ more negative than that of the $SO_2 + O_3^- \rightarrow SO_3^- + O_2$ reaction at similar conditions. Given that the intermediate steps of Reaction (R4) are significantly

fast, this reaction is believed to be an important process in most environments of SO_2 ion-induced oxidation to SO_3^- or more oxidized species. The limiting step in the process of Reaction (R4) is Reaction (R4c) for which an energy barrier has to be overcome before the products are released.

SO_3^- is an identified stable ion detected in the atmosphere and in experiments (Ehn et al., 2010; Kirkby et al., 2011, 2016). The chemical fate of SO_3^- is fundamentally different from that of SO_3 that forms H_2SO_4 by hydration. Likely outcomes of SO_3^- are hydrolysis, electron transfer by collision with O_3, reaction with O_2 and H_2O, and, possibly, radicals, according to the following equations:

$$SO_3^- + H_2O \rightarrow SO_3^- \cdots H_2O \rightarrow H_2SO_4 + e^- \quad \text{(R5)}$$

$$SO_3^- + O_3 \rightarrow SO_3 + O_3^- \quad \text{(R6)}$$

$$SO_3^- + O_2 + H_2O \rightarrow HSO_4^- + HO_2 \quad \text{(R7)}$$

$$SO_3^- + OH \rightarrow HSO_4^-. \quad \text{(R8)}$$

Fehsenfeld and Ferguson showed that H_2SO_4 formation could occur in the $SO_3^- \cdots H_2O$ cluster, releasing a free electron (Reaction R5) (Fehsenfeld and Ferguson, 1974). Owing to the high electron affinity of O_3 relative to SO_3 (Rothe et al., 1975), the electron can transfer from SO_3^- to O_3 and lead to the formation of SO_3, the precursor for sulfuric acid in the atmosphere. Moreover, the free electron released and the O_3^- formed in Reactions (R5) and (R6), respectively, are potential triggers of new SO_2 oxidations with implication for aerosol formation (Svensmark et al., 2007; Enghoff and Svensmark, 2008; Bork et al., 2013). Reactions (R7) and (R8) are potential outcomes for SO_3^- as well, forming the highly stable HSO_4^- species that would terminate the oxidation process of SO_2 initiated by a free electron. Reactions (R5)–(R8) are likely competitive processes upon SO_3^- formation in the gas phase, and their different rates would determine the number of SO_2 oxidations induced by a free electron. However, they have no other fate than HSO_4^- or H_2SO_4, the most oxidized sulfur species in the atmosphere, which both share many properties and play a central role in atmospheric particle formation.

Experimental studies have shown that in atmospheres heavily enriched in SO_2 and O_3, a free electron could initiate SO_2 oxidation and induce the formation of $\sim 10^7$ cm^{-3} sulfates in the absence of UV light, clearly indicating the importance of other ionic SO_2 oxidation mechanisms than UV-induced oxidation (Enghoff and Svensmark, 2008). To evaluate the importance of the mechanism presented in this study in the formation of sulfate, it is necessary to identify the scavengers that terminate the SO_2 oxidation initiated by O_2^-. Possible scavengers include radicals, NO_x, acids, cations, and other particles. The main ones are likely NO_x, OH, HO_2, and organic acids, which lead to the formation of the stable NO_3^-, HSO_4^-, and CO_3^- species. If the ion concentration was known, the contribution of Reaction (R4) to H_2SO_4 formation could be determined by comparing its formation rates from ionic and electrically neutral mechanisms. Alternatively, it can be assumed that Reaction (R4) is terminated when the ion cluster hits a scavenger. The free electron which acts as a catalyst is then scavenged. The average catalytic turnover number (TON) is defined as follows (Kozuch and Martin, 2012):

$$\text{TON} = \frac{\text{concentration of limiting reacted molecules}}{\text{concentration of the catalyst}}. \quad (8)$$

The concentration of the catalyst can be approximated to the concentration of the scavengers and, considering that at most atmospheric conditions $[O_3] > [SO_2]$, SO_2 is the limiting species in Reaction (R4). Equation (8) can then be rewritten as

$$\text{TON} \approx \frac{[SO_2]}{[OH] + [HO_2] + [NO_x] + [\text{organic acids}]}. \quad (9)$$

The catalytic efficiency of SO_2 ion-induced oxidation is then given as

$$J_{\text{ion}} = k_{\text{ion}} \times \text{TON}, \quad (10)$$

where k_{ion} is the ion production rate. Depending on the tropospheric temperature and altitude, measurements at the Cosmics Leaving Outdoor Droplets chamber at CERN found $k_{\text{ion}} = 2$–$100\,\text{cm}^{-3}\,\text{s}^{-1}$, covering the typical ionization range in the troposphere (Franchin et al., 2015). We assume nearly pristine conditions with $[SO_2] = 5\,\text{ppb} = 1.2 \times 10^{11}$ molecule cm^{-3}, $[NO_x] = 200\,\text{ppt} = 4.9 \times 10^9$ molecule cm^{-3}, $[OH] = 5.0 \times 10^5$ molecule cm^{-3} (day and night average), and $[HO_2] = 10^8$ molecule cm^{-3} (Dusanter et al., 2009; Holland et al., 2003). Noting that formic acid and acetic acid are the most abundant organic acids in the atmosphere, their concentrations are considered in Eq. (9) as representative examples for organic acids, [organic acids] $= 110\,\text{ppt} = 2.7 \times 10^9$ molecule cm^{-3} (Le Breton et al., 2012; Baasandorj et al., 2015). We then determine J_{ion} in the range 3.2×10^1–$1.6 \times 10^3\,\text{cm}^{-3}\,\text{s}^{-1}$. The rate of the UV-induced SO_2 oxidation by OH is

$$J_{\text{UV}} = k_{\text{UV}} \times [SO_2] \times [OH]. \quad (11)$$

With $k_{\text{UV}} = 1.3 \times 10^{-12}\,\text{cm}^3\,\text{molecule}^{-1}\,\text{s}^{-1}$ (Atkinson et al., 2004), $J_{\text{UV}} = 7.9 \times 10^4$ molecule cm^{-3} s^{-1}, the proportion of H_2SO_4 formed from ion-induced oxidation can be estimated from the following equation:

$$\frac{[H_2SO_4]_{\text{ion}}}{[H_2SO_4]_{\text{total}}} = \frac{J_{\text{ion}}}{J_{\text{UV}} + J_{\text{ion}}}. \quad (12)$$

We find that the contribution of ion-induced SO_2 oxidation to H_2SO_4 formation can range from 0.1 % to 2.0 % of the total formation rate. This estimate could be improved by also considering the rate of SO_2 oxidation by Criegee intermediates, another important channel for H_2SO_4 formation.

4 Conclusions

This study highlights the role of the superoxide ions (O_2^-) in SO_2 oxidation. Our previous study demonstrated that SO_2 interacts with O_2^- and forms O_2SOO^-, whose atmospheric fate remains unelucidated (Tsona et al., 2014). In this study, we used ab initio calculations to assess the chemical fate of O_2SOO^- by collisions with O_3. Regardless of the presence of water, two main mechanisms are observed, leading to fundamentally different products. The first mechanism is characterized by electron transfer followed by O_2SOO^- decomposition, leading to O_3^- formation and releasing SO_2. The chemistry of $SO_2 + O_3^-$ has been explored elsewhere. The second mechanism is characterized by SO_2 oxidation and proceeds through formation of a pre-reactive complex that subsequently reacts to form the products by overcoming a relatively low energy barrier. The overall reaction, $O_2^- + SO_2 + O_3 \rightarrow SO_3^- + 2O_2$, is faster and more energetically favorable than the $SO_2 + O_3^- \rightarrow SO_3^- + O_2$ reaction, thereby highlighting the positive role of O_2^- in SO_2 ionic oxidation. Hence, the two reactions may compete in chamber experiments and in the atmosphere.

While for the electron transfer and O_2SOO^- decomposition process the reaction is hindered by the presence of water, the oxidation reaction is catalyzed instead, as the rate constant is increased by 6 orders of magnitude with the presence of water. Weighing the rate constants of unhydrated and monohydrated reactions to the equilibrium concentrations of hydrates of corresponding pre-reactive complexes leads to the net rate constant of 4.0×10^{-11} cm^3 molecule^{-1} s^{-1} at 298 K for the oxidation reaction. Hence, this reaction proceeds nearly at collision rate. The main species (SO_3^-) in the end products of the studied reaction has been proved to form both in the atmosphere and in experiments, whereby it definitely plays a role in atmospheric sulfur chemistry and particle formation. The contribution of this mechanism to the total atmospheric sulfuric acid formation is estimated. The studied reaction further deepens the understanding of ion-induced SO_2 oxidation, with implications for aerosol formation.

Data availability. The results presented in this article are from Gaussian calculations, exclusively, and they are obtained by exploiting the output files from these calculations. These files can be obtained by contacting the authors.

Supplement. The supplement related to this article is available online at: https://doi.org/10.5194/acp-19-649-2019-supplement.

Author contributions. NTT and LD designed the work. NTT performed all calculations and analyzed the data. NTT wrote the whole manuscript and LD edited it.

Competing interests. The authors declare that they have no conflict of interest.

Acknowledgements. This work was supported by the National Natural Science Foundation of China (21707080, 91644214), the Postdoctoral Science Foundation of China (2017M612276), the Shandong Natural Science Fund for Distinguished Young Scholars (JQ201705), and the International Postdoctoral Exchange Fellowship Program. We acknowledge the High-Performance Computing Center of Shandong University for providing the computational resources.

Edited by: Sergey A. Nizkorodov
Reviewed by: two anonymous referees

References

Atkinson, R., Baulch, D. L., Cox, R. A., Crowley, J. N., Hampson, R. F., Hynes, R. G., Jenkin, M. E., Rossi, M. J., and Troe, J.: Evaluated kinetic and photochemical data for atmospheric chemistry: Volume I – gas phase reactions of O_x, HO_x, NO_x and SO_x species, Atmos. Chem. Phys., 4, 1461–1738, https://doi.org/10.5194/acp-4-1461-2004, 2004.

Baasandorj, M., Millet, D. B., Hu, L., Mitroo, D., and Williams, B. J.: Measuring acetic and formic acid by proton-transfer-reaction mass spectrometry: sensitivity, humidity dependence, and quantifying interferences, Atmos. Meas. Tech., 8, 1303–1321, https://doi.org/10.5194/amt-8-1303-2015, 2015.

Bader, R. F. W.: A Bond Path: A Universal Indicator of Bonded Interactions, J. Phys. Chem. A, 102, 7314–7323, https://doi.org/10.1021/jp981794v, 1998.

Bork, N., Kurtén, T., Enghoff, M., Pedersen, J. O. P., Mikkelsen, K. V., and Svensmark, H.: Ab initio studies of $O_2^-(H_2O)_n$ and $O_3^-(H_2O)_n$ anionic molecular clusters, $n = 12$, Atmos. Chem. Phys., 11, 7133–7142, https://doi.org/10.5194/acp-11-7133-2011, 2011.

Bork, N., Kurtén, T., Enghoff, M., Pedersen, J. O. P., Mikkelsen, K. V., and Svensmark, H.: Structures and reaction rates of the gaseous oxidation of SO_2 by an $O_3^-(H_2O)_{0-5}$ cluster – a density functional theory investigation, Atmos. Chem. Phys., 12, 3639–3652, https://doi.org/10.5194/acp-12-3639-2012, 2012.

Bork, N., Kurtén, T., and Vehkamäki, H.: Exploring the atmospheric chemistry of $O_2SO_3^-$ and assessing the maximum turnover number of ion-catalysed H_2SO_4 formation, Atmos. Chem. Phys., 13, 3695–3703, https://doi.org/10.5194/acp-13-3695-2013, 2013.

Buttar, D. and Hirst, D. M.: Ab initio quantum chemistry study of the gas-phase reaction of ClO with HO_2, J. Chem. Soc. Faraday Trans., 90, 1811–1817, https://doi.org/10.1039/FT9949001811, 1994.

Caffrey, P., Hoppel, W., Frick, G., Pasternack, L., Fitzgerald, J., Hegg, D., Gao, S., Leaitch, R., Shantz, N., Albrechcinski, T., and Ambrusko, J.: In-cloud oxidation of SO_2 by O_3 and H_2O_2: Cloud chamber measurements and modeling of particle growth, J. Geophys. Res.-Atmos., 106, 27587–27601, https://doi.org/10.1029/2000jd900844, 2001.

Cheng, Y., Zheng, G., Wei, C., Mu, Q., Zheng, B., Wang, Z., Gao, M., Zhang, Q., He, K., Carmichael, G., Pöschl, U., and Su,

H.: Reactive nitrogen chemistry in aerosol water as a source of sulfate during haze events in China, Sci. Adv., 2, e1601530, https://doi.org/10.1126/sciadv.1601530, 2016.

Drougas, E. and Kosmas, A. M.: Computational studies of (HIO_3) isomers and the $HO_2 + IO$ reaction pathways, J. Phys. Chem. A, 109, 3887–3892, https://doi.org/10.1021/jp044197j, 2005.

Dunning Jr., T. H., Peterson, K. A., and Wilson, A. K.: Gaussian basis sets for use in correlated molecular calculations. X. The atoms aluminum through argon revisited, J. Chem. Phys., 114, 9244–9253, https://doi.org/10.1063/1.1367373, 2001.

Dusanter, S., Vimal, D., Stevens, P. S., Volkamer, R., Molina, L. T., Baker, A., Meinardi, S., Blake, D., Sheehy, P., Merten, A., Zhang, R., Zheng, J., Fortner, E. C., Junkermann, W., Dubey, M., Rahn, T., Eichinger, B., Lewandowski, P., Prueger, J., and Holder, H.: Measurements of OH and HO_2 concentrations during the MCMA-2006 field campaign – Part 2: Model comparison and radical budget, Atmos. Chem. Phys., 9, 6655–6675, https://doi.org/10.5194/acp-9-6655-2009, 2009.

Ehn, M., Junninen, H., Petäjä, T., Kurtén, T., Kerminen, V.-M., Schobesberger, S., Manninen, H., Ortega, I., Vehkamäki, H., and Kulmala, M.: Composition and temporal behavior of ambient ions in the boreal forest, Atmos. Chem. Phys., 10, 8513–8530, https://doi.org/10.5194/acp-10-8513-2010, 2010.

Eisele, F. L., Lovejoy, E. R., Kosciuch, E., Moore, K. F., Mauldin III, R. L., Smith, J. N., McMurry, P. H., and Iida, K.: Negative atmospheric ions and their potential role in ion-induced nucleation, J. Geophys. Res.-Atmos., 111, D04305, https://doi.org/10.1029/2005jd006568, 2006.

Elm, J., Bilde, M., and Mikkelsen, K. V.: Assessment of Density Functional Theory in Predicting Structures and Free Energies of Reaction of Atmospheric Prenucleation Clusters, J. Chem. Theory Comput., 8, 2071–2077, https://doi.org/10.1021/ct300192p, 2012.

Elm, J., Bilde, M., and Mikkelsen, K. V.: Assessment of binding energies of atmospherically relevant clusters, Phys. Chem. Chem. Phys., 15, 16442–16445, https://doi.org/10.1039/c3cp52616j, 2013a.

Elm, J., Bilde, M., and Mikkelsen, K. V.: Influence of Nucleation Precursors on the Reaction Kinetics of Methanol with the OH Radical, J. Phys. Chem. A, 117, 6695–6701, https://doi.org/10.1021/jp4051269, 2013b.

Enghoff, M. and Svensmark, H.: The role of atmospheric ions in aerosol nucleation – a review, Atmos. Chem. Phys., 8, 4911–4923, https://doi.org/10.5194/acp-8-4911-2008, 2008.

Enghoff, M. B., Bork, N., Hattori, S., Meusinger, C., Nakagawa, M., Pedersen, J. O. P., Danielache, S., Ueno, Y., Johnson, M. S., Yoshida, N., and Svensmark, H.: An isotopic analysis of ionising radiation as a source of sulphuric acid, Atmos. Chem. Phys., 12, 5319–5327, https://doi.org/10.5194/acp-12-5319-2012, 2012.

Fahey, D., Böhringer, H., Fehsenfeld, F., and Ferguson, E.: Reaction rate constants for $O_2^-(H_2O)_n$ ions $n = 0$ to 4, with O_3, NO, SO_2, and CO_2, J. Chem. Phys., 76, 1799–1805, https://doi.org/10.1063/1.443220, 1982.

Fehsenfeld, F. and Ferguson, E.: Laboratory studies of negative ion reactions with atmospheric trace constituents, J. Chem. Phys., 61, 3181–3193, https://doi.org/10.1063/1.1682474, 1974.

Franchin, A., Ehrhart, S., Leppä, J., Nieminen, T., Gagné, S., Schobesberger, S., Wimmer, D., Duplissy, J., Riccobono, F., Dunne, E. M., Rondo, L., Downard, A., Bianchi, F., Kupc, A., Tsagkogeorgas, G., Lehtipalo, K., Manninen, H. E., Almeida, J., Amorim, A., Wagner, P. E., Hansel, A., Kirkby, J., Kürten, A., Donahue, N. M., Makhmutov, V., Mathot, S., Metzger, A., Petäjä, T., Schnitzhofer, R., Sipilä, M., Stozhkov, Y., Tome, A., Kerminen, V. M., Carslaw, K., Curtius, J., Baltensperger, U., and Kulmala, M.: Experimental investigation of ion-ion recombination under atmospheric conditions, Atmos. Chem. Phys., 15, 7203–7216, https://doi.org/10.5194/acp-15-7203-2015, 2015.

Frisch, M. J., Trucks, G. W., Schlegel, H. B., Scuseria, G. E., Robb, M. A., Cheeseman, J. R., Scalmani, G., Barone, V., Mennucci, B., Petersson, G. A., Nakatsuji, H., Caricato, M., Li, X., Hratchian, H. P., Izmaylov, A. F., Bloino, J., Zheng, G., Sonnenberg, J. L., Hada, M., Ehara, M., Toyota, K., Fukuda, R., Hasegawa, J., Ishida, M., Nakajima, T., Honda, Y., Kitao, O., Nakai, H., Vreven, T., Montgomery Jr., J. A., Peralta, J. E., Ogliaro, F., Bearpark, M. J., Heyd, J., Brothers, E. N., Kudin, K. N., Staroverov, V. N., Kobayashi, R., Normand, J., Raghavachari, K., Rendell, A. P., Burant, J. C., Iyengar, S. S., Tomasi, J., Cossi, M., Rega, N., Millam, N. J., Klene, M., Knox, J. E., Cross, J. B., Bakken, V., Adamo, C., Jaramillo, J., Gomperts, R., Stratmann, R. E., Yazyev, O., Austin, A. J., Cammi, R., Pomelli, C., Ochterski, J. W., Martin, R. L., Morokuma, K., Zakrzewski, V. G., Voth, G. A., Salvador, P., Dannenberg, J. J., Dapprich, S., Daniels, A. D., Farkas, Ö., Foresman, J. B., J. Ortiz, V., Cioslowski, J., and Fox, D. J.: Gaussian 09, Revision E.01, Gaussian, Inc., Wallingford, CT, USA, 2013.

Fukui, K.: The path of chemical reactions-the IRC approach, Acc. Chem. Res., 14, 363–368, https://doi.org/10.1021/ar00072a001, 1981.

Georgievskii, Y. and Klippenstein, S. J.: Long-range transition state theory, J. Chem. Phys., 122, 194103, https://doi.org/10.1063/1.1899603, 2005.

Greenwald, E. E., North, S. W., Georgievskii, Y., and Klippenstein, S. J.: A two transition state model for radical-molecule reactions: A case study of the addition of OH to C_2H_4, J. Phys. Chem. A, 109, 6031–6044, https://doi.org/10.1021/jp058041a, 2005.

Harris, E., Sinha, B., Hoppe, P., Crowley, J. N., Ono, S., and Foley, S.: Sulfur isotope fractionation during oxidation of sulfur dioxide: gas-phase oxidation by OH radicals and aqueous oxidation by H_2O_2, O_3 and iron catalysis, Atmos. Chem. Phys., 12, 407–423, https://doi.org/10.5194/acp-12-407-2012, 2012.

Harris, E., Sinha, B., van Pinxteren, D., Tilgner, A., Fomba, K. W., Schneider, J., Roth, A., Gnauk, T., Fahlbusch, B., Mertes, S., Lee, T., Collett, J., Foley, S., Borrmann, S., Hoppe, P., and Herrmann, H.: Enhanced Role of Transition Metal Ion Catalysis During In-Cloud Oxidation of SO_2, Science, 340, 727–730, https://doi.org/10.1126/science.1230911, 2013.

Hegg, D. A., Majeed, R., Yuen, P. F., Baker, M. B., and Larson, T. V.: The impacts of SO_2 oxidation in cloud drops and in haze particles on aerosol light scattering and CCN activity, Geophys. Res. Lett., 23, 2613–2616, https://doi.org/10.1029/96gl02419, 1996.

Henkelman, G., Arnaldsson, A., and Jónsson, H.: A fast and robust algorithm for Bader decomposition of charge density, Comput. Mater. Sci., 36, 354–360, https://doi.org/10.1016/j.commatsci.2005.04.010, 2006.

Hirsikko, A., Nieminen, T., Gagné, S., Lehtipalo, K., Manninen, H. E., Ehn, M., Hõrrak, U., Kerminen, V. M., Laakso, L., McMurry, P. H., Mirme, A., Mirme, S., Petäjä, T., Tammet, H., Vakkari, V., Vana, M., and Kulmala, M.: Atmospheric ions and nucle-

ation: a review of observations, Atmos. Chem. Phys., 11, 767–798, https://doi.org/10.5194/acp-11-767-2011, 2011.

Holland, F., Hofzumahaus, A., Schafer, R., Kraus, A., and Patz, H. W.: Measurements of OH and HO_2 radical concentrations and photolysis frequencies during BERLIOZ, J. Geophys. Res.-Atmos., 108, 8246, https://doi.org/10.1029/2001jd001393, 2003.

Hoyle, C. R., Fuchs, C., Järvinen, E., Saathoff, H., Dias, A., El Haddad, I., Gysel, M., Coburn, S. C., Tröstl, J., Bernhammer, A. K., Bianchi, F., Breitenlechner, M., Corbin, J. C., Craven, J., Donahue, N. M., Duplissy, J., Ehrhart, S., Frege, C., Gordon, H., Höppel, N., Heinritzi, M., Kristensen, T. B., Molteni, U., Nichman, L., Pinterich, T., Prévôt, A. S. H., Simon, M., Slowik, J. G., Steiner, G., Tomé, A., Vogel, A. L., Volkamer, R., Wagner, A. C., Wagner, R., Wexler, A. S., Williamson, C., Winkler, P. M., Yan, C., Amorim, A., Dommen, J., Curtius, J., Gallagher, M. W., Flagan, R. C., Hansel, A., Kirkby, J., Kulmala, M., Möhler, O., Stratmann, F., Worsnop, D. R., and Baltensperger, U.: Aqueous phase oxidation of sulphur dioxide by ozone in cloud droplets, Atmos. Chem. Phys., 16, 1693–1712, https://doi.org/10.5194/acp-16-1693-2016, 2016.

Hvelplund, P., Pedersen, J. O. P., Stochkel, K., Enghoff, M. B., and Kurten, T.: Experimental studies of the formation of cluster ions formed by corona discharge in an atmosphere containing SO_2, NH_3, and H_2O, Int. J. Mass Spectrom., 341, 1–6, https://doi.org/10.1016/j.ijms.2013.03.001, 2013.

Kirkby, J., Curtius, J., Almeida, J., Dunne, E., Duplissy, J., Ehrhart, S., Franchin, A., Gagné, S., Ickes, L., Kürten, A., Kupc, A., Metzger, A., Riccobono, F., Rondo, L., Schobesberger, S., Tsagkogeorgas, G., Wimmer, D., Amorim, A., Bianchi, F., Breitenlechner, M., David, A., Dommen, J., Downard, A., Ehn, M., Flagan, R. C., Haider, S., Hansel, A., Hauser, D., Jud, W., Junninen, H., Kreissl, F., Kvashin, A., Laaksonen, A., Lehtipalo, K., Lima, J., Lovejoy, E. R., Makhmutov, V., Mathot, S., Mikkila, J., Minginette, P., Mogo, S., Nieminen, T., Onnela, A., Pereira, P., Petäjä, T., Schnitzhofer, R., Seinfeld, J. H., Sipilä, M., Stozhkov, Y., Stratmann, F., Tomé, A., Vanhanen, J., Viisanen, Y., Vrtala, A., Wagner, P. E., Walther, H., Weingartner, E., Wex, H., Winkler, P. M., Carslaw, K. S., Worsnop, D. R., Baltensperger, U., and Kulmala, M.: Role of sulphuric acid, ammonia and galactic cosmic rays in atmospheric aerosol nucleation, Nature, 476, 429–433, https://doi.org/10.1038/nature10343, 2011.

Kirkby, J., Duplissy, J., Sengupta, K., Frege, C., Gordon, H., Williamson, C., Heinritzi, M., Simon, M., Yan, C., Almeida, J., Tröstl, J., Nieminen, T., Ortega, I. K., Wagner, R., Adamov, A., Amorim, A., Bernhammer, A.-K., Bianchi, F., Breitenlechner, M., Brilke, S., Chen, X., Craven, J., Dias, A., Ehrhart, S., Flagan, R. C., Franchin, A., Fuchs, C., Guida, R., Hakala, J., Hoyle, C. R., Jokinen, T., Junninen, H., Kangasluoma, J., Kim, J., Krapf, M., Kürten, A., Laaksonen, A., Lehtipalo, K., Makhmutov, V., Mathot, S., Molteni, U., Onnela, A., Peräkylä, O., Piel, F., Petäjä, T., Praplan, A. P., Pringle, K., Rap, A., Richards, N. A. D., Riipinen, I., Rissanen, M. P., Rondo, L., Sarnela, N., Schobesberger, S., Scott, C. E., Seinfeld, J. H., Sipilä, M., Steiner, G., Stozhkov, Y., Stratmann, F., Tomé, A., Virtanen, A., Vogel, A. L., Wagner, A. C., Wagner, P. E., Weingartner, E., Wimmer, D., Winkler, P. M., Ye, P., Zhang, X., Hansel, A., Dommen, J., Donahue, N. M., Worsnop, D. R., Baltensperger, U., Kulmala, M., Carslaw, K. S., and Curtius, J.: Ion-induced nucleation of pure biogenic particles, Nature, 533, 521–526, https://doi.org/10.1038/nature17953, 2016.

Klippenstein, S. J., Khundkar, L. R., Zewail, A. H., and Marcus, R. A.: Application of unimolecular reaction-rate theory for highly flexible transition-states to the dissociation of NCNO into NC and NO, J. Chem. Phys., 89, 4761–4770, https://doi.org/10.1063/1.455670, 1988.

Kozuch, S. and Martin, J. M. L.: "Turning Over" Definitions in Catalytic Cycles, Acs Catalysis, 2, 2787–2794, https://doi.org/10.1021/cs3005264, 2012.

Kuang, C., McMurry, P. H., McCormick, A. V., and Eisele, F. L.: Dependence of nucleation rates on sulfuric acid vapor concentration in diverse atmospheric locations, J. Geophys. Res.-Atmos., 113, D10209, https://doi.org/10.1029/2007jd009253, 2008.

Kulmala, M., Pirjola, L., and Mäkelä, J. M.: Stable sulphate clusters as a source of new atmospheric particles, Nature, 404, 66–69, https://doi.org/10.1038/35003550, 2000.

Kupiainen-Määttä, O., Olenius, T., Kurtén, T., and Vehkamäki, H.: CIMS sulfuric acid detection efficiency enhanced by amines due to higher dipole moments: a computational study, J. Phys. Chem. A, 117, 14109–14119, https://doi.org/10.1021/jp4049764, 2013.

Larson, L. J., Kuno, M., and Tao, F.-M.: Hydrolysis of sulfur trioxide to form sulfuric acid in small water clusters, J. Chem. Phys., 112, 8830–8838, https://doi.org/10.1063/1.481532, 2000.

Le Breton, M., McGillen, M. R., Muller, J. B. A., Bacak, A., Shallcross, D. E., Xiao, P., Huey, L. G., Tanner, D., Coe, H., and Percival, C. J.: Airborne observations of formic acid using a chemical ionization mass spectrometer, Atmos. Meas. Tech., 5, 3029–3039, https://doi.org/10.5194/amt-5-3029-2012, 2012.

Manninen, H. E., Nieminen, T., Asmi, E., Gagné, S., Häkkinen, S., Lehtipalo, K., Aalto, P., Vana, M., Mirme, A., Mirme, S., Hõrrak, U., Plass-Dülmer, C., Stange, G., Kiss, G., Hoffer, A., Törő, N., Moerman, M., Henzing, B., de Leeuw, G., Brinkenberg, M., Kouvarakis, G. N., Bougiatioti, A., Mihalopoulos, N., O'Dowd, C., Ceburnis, D., Arneth, A., Svenningsson, B., Swietlicki, E., Tarozzi, L., Decesari, S., Facchini, M. C., Birmili, W., Sonntag, A., Wiedensohler, A., Boulon, J., Sellegri, K., Laj, P., Gysel, M., Bukowiecki, N., Weingartner, E., Wehrle, G., Laaksonen, A., Hamed, A., Joutsensaari, J., Petäjä, T., Kerminen, V. M., and Kulmala, M.: EUCAARI ion spectrometer measurements at 12 European sites – analysis of new particle formation events, Atmos. Chem. Phys., 10, 7907–7927, https://doi.org/10.5194/acp-10-7907-2010, 2010.

Mauldin III, R. L., Berndt, T., Sipilä, M., Paasonen, P., Petäjä, T., Kim, S., Kurtén, T., Stratmann, F., Kerminen, V.-M., and Kulmala, M.: A new atmospherically relevant oxidant of sulphur dioxide, Nature, 488, 193–196, https://doi.org/10.1038/nature11278, 2012.

Möhler, O., Reiner, T., and Arnold, F.: The formation of SO_5^- by gas phase ion–molecule reactions, J. Chem. Phys., 97, 8233–8239, https://doi.org/10.1063/1.463394, 1992.

Nagato, K., Kim, C. S., Adachi, M., and Okuyama, K.: An experimental study of ion-induced nucleation using a drift tube ion, mobility spectrometer/mass spectrometer and a cluster-differential mobility analyzer/Faraday cup electrometer, J. Aerosol Sci., 36, 1036–1049, https://doi.org/10.1016/j.jaerosci.2004.12.006, 2005.

Nieminen, T., Manninen, H., Sihto, S.-L., Yli-Juuti, T., Mauldin III, R. L., Petäjä, T., Riipinen, I., Kerminen, V.-M., and Kulmala, M.: Connection of sulfuric acid to atmospheric nucleation in boreal forest, Environ. Sci. Technol., 43, 4715–4721, https://doi.org/10.1021/es803152j, 2009.

Noziere, B., Ekstrom, S., Alsberg, T., and Holmstrom, S.: Radical-initiated formation of organosulfates and surfactants in atmospheric aerosols, Geophys. Res. Lett., 37, L05806, https://doi.org/10.1029/2009gl041683, 2010.

Peng, C., Ayala, P. Y., Schlegel, H. B., and Frisch, M. J.: Using redundant internal coordinates to optimize equilibrium geometries and transition states, J. Comput. Chem., 17, 49–56, 1996.

Purvis, G. D. and Bartlett, R. J.: A full coupled-cluster singles and doubles model – the inclusion of disconnected triples, J. Chem. Phys., 76, 1910–1918, https://doi.org/10.1063/1.443164, 1982.

Rothe, E. W., Tang, S. Y., and Reck, G. P.: Measurement of electron affinities of O_3, SO_2, and SO_3 by collisional ionization, J. Chem. Phys., 62, 3829–3831, https://doi.org/10.1063/1.430941, 1975.

Schindelka, J., Iinuma, Y., Hoffmann, D., and Herrmann, H.: Sulfate radical-initiated formation of isoprene-derived organosulfates in atmospheric aerosols, Faraday Discuss., 165, 237–259, https://doi.org/10.1039/c3fd00042g, 2013.

Schweitzer, C. and Schmidt, R.: Physical mechanisms of generation and deactivation of singlet oxygen, Chem. Rev., 103, 1685–1757, https://doi.org/10.1021/cr010371d, 2003.

Seinfeld, J. H. and Pandis, S. N.: Atmospheric Chemistry and Physics: From Air Pollution to Climate Change, 3rd Edn., John Wiley & Sons, Inc., New Jersey, 2016.

Sipilä, M., Berndt, T., Petäjä, T., Brus, D., Vanhanen, J., Stratmann, F., Patokoski, J., Mauldin III, R. L., Hyvarinen, A.-P., Lihavainen, H., and Kulmala, M.: The Role of Sulfuric Acid in Atmospheric Nucleation, Science, 327, 1243–1246, https://doi.org/10.1126/science.1180315, 2010.

Su, T. and Chesnavich, W. J.: Parametrization of the ion-polar molecule collision rate-constant by trajectory calculations, J. Chem. Phys., 76, 5183–5185, https://doi.org/10.1063/1.442828, 1982.

Surratt, J. D., Lewandowski, M., Offenberg, J. H., Jaoui, M., Kleindienst, T. E., Edney, E. O., and Seinfeld, J. H.: Effect of acidity on secondary organic aerosol formation from isoprene, Environ. Sci. Technol., 41, 5363–5369, https://doi.org/10.1021/es0704176, 2007.

Surratt, J. D., Gomez-Gonzalez, Y., Chan, A. W. H., Vermeylen, R., Shahgholi, M., Kleindienst, T. E., Edney, E. O., Offenberg, J. H., Lewandowski, M., Jaoui, M., Maenhaut, W., Claeys, M., Flagan, R. C., and Seinfeld, J. H.: Organosulfate formation in biogenic secondary organic aerosol, J. Phys. Chem. A, 112, 8345–8378, https://doi.org/10.1021/jp802310p, 2008.

Svensmark, H., Pedersen, J. O. P., Marsh, N. D., Enghoff, M. B., and Uggerhoj, U. I.: Experimental evidence for the role of ions in particle nucleation under atmospheric conditions, Proc. Roy. Soc. A, 463, 385–396, https://doi.org/10.1098/rspa.2006.1773, 2007.

Tang, W., Sanville, E., and Henkelman, G.: A grid-based Bader analysis algorithm without lattice bias, J. Phys. Condens. Matter, 21, 084204, https://doi.org/10.1088/0953-8984/21/8/084204, 2009.

Tsona, N., Bork, N., and Vehkamäki, H.: Exploring the chemical fate of the sulfate radical anion by reaction with sulfur dioxide in the gas phase, Atmos. Chem. Phys., 15, 495–503, https://doi.org/10.5194/acp-15-495-2015, 2015.

Tsona, N. T., Bork, N., and Vehkamäki, H.: On the gas-phase reaction between SO_2 and $O_2^-(H_2O)_{0-3}$ clusters – an ab initio study, Phys. Chem. Chem. Phys., 16, 5987–5992, https://doi.org/10.1039/c3cp54715a, 2014.

Tsona, N. T., Bork, N., Loukonen, V., and Vehkamäki, H.: A Closure Study of the Reaction between Sulfur Dioxide and the Sulfate Radical Ion from First-Principles Molecular Dynamics Simulations, J. Phys. Chem. A, 120, 1046–1050, https://doi.org/10.1021/acs.jpca.5b12395, 2016.

Tsona, N. T., Li, J., and Du, L.: From O_2^--Initiated SO_2 oxidation to sulfate formation in the gas-phase, J. Phys. Chem. A, 122, 5781–5788, https://doi.org/10.1021/acs.jpca.8b03381, 2018.

Vereecken, L., Harder, H., and Novelli, A.: The reaction of Criegee intermediates with NO, RO_2, and SO_2, and their fate in the atmosphere, Phys. Chem. Chem. Phys., 14, 14682–14695, https://doi.org/10.1039/c2cp42300f, 2012.

Wagner, R., Yan, C., Lehtipalo, K., Duplissy, J., Nieminen, T., Kangasluoma, J., Ahonen, L. R., Dada, L., Kontkanen, J., Manninen, H. E., Dias, A., Amorim, A., Bauer, P. S., Bergen, A., Bernhammer, A. K., Bianchi, F., Brilke, S., Mazon, S. B., Chen, X., Draper, D. C., Fischer, L., Frege, C., Fuchs, C., Garmash, O., Gordon, H., Hakala, J., Heikkinen, L., Heinritzi, M., Hofbauer, V., Hoyle, C. R., Kirkby, J., Kürten, A., Kvashnin, A. N., Laurila, T., Lawler, M. J., Mai, H., Makhmutov, V., Mauldin Iii, R. L., Molteni, U., Nichman, L., Nie, W., Ojdanic, A., Onnela, A., Piel, F., Quéléver, L. L. J., Rissanen, M. P., Sarnela, N., Schallhart, S., Sengupta, K., Simon, M., Stolzenburg, D., Stozhkov, Y., Tröstl, J., Viisanen, Y., Vogel, A. L., Wagner, A. C., Xiao, M., Ye, P., Baltensperger, U., Curtius, J., Donahue, N. M., Flagan, R. C., Gallagher, M., Hansel, A., Smith, J. N., Tomé, A., Winkler, P. M., Worsnop, D., Ehn, M., Sipilä, M., Kerminen, V. M., Petäjä, T., and Kulmala, M.: The role of ions in new particle formation in the CLOUD chamber, Atmos. Chem. Phys., 17, 15181–15197, https://doi.org/10.5194/acp-17-15181-2017, 2017.

Wang, G., Zhang, R., Gomez, M. E., Yang, L., Levy Zamora, M., Hu, M., Lin, Y., Peng, J., Guo, S., Meng, J., Li, J., Cheng, C., Hu, T., Ren, Y., Wang, Y., Gao, J., Cao, J., An, Z., Zhou, W., Li, G., Wang, J., Tian, P., Marrero-Ortiz, W., Secrest, J., Du, Z., Zheng, J., Shang, D., Zeng, L., Shao, M., Wang, W., Huang, Y., Wang, Y., Zhu, Y., Li, Y., Hu, J., Pan, B., Cai, L., Cheng, Y., Ji, Y., Zhang, F., Rosenfeld, D., Liss, P. S., Duce, R. A., Kolb, C. E., and Molina, M. J.: Persistent sulfate formation from London Fog to Chinese haze, P. Natl. Acad. Sci. USA, 113, 13630, https://doi.org/10.1073/pnas.1616540113, 2016.

Welz, O., Savee, J. D., Osborn, D. L., Vasu, S. S., Percival, C. J., Shallcross, D. E., and Taatjes, C. A.: Direct kinetic measurements of Criegee intermediate (CH_2OO) formed by reaction of CH_2I with O_2, Science, 335, 204–207, https://doi.org/10.1126/science.1213229, 2012.

Yan, C., Dada, L., Rose, C., Jokinen, T., Nie, W., Schobesberger, S., Junninen, H., Lehtipalo, K., Sarnela, N., Makkonen, U., Garmash, O., Wang, Y., Zha, Q., Paasonen, P., Bianchi, F., Sipilä, M., Ehn, M., Petäjä, T., Kerminen, V. M., Worsnop, D. R., and Kulmala, M.: The role of H_2SO_4–NH_3 anion clusters in ion-induced aerosol nucleation mechanisms in the boreal forest, Atmos. Chem. Phys., 18, 13231–13243, https://doi.org/10.5194/acp-18-13231-2018, 2018.

Yu, F.: From molecular clusters to nanoparticles: second-generation ion-mediated nucleation model, Atmos. Chem. Phys., 6, 5193–5211, https://doi.org/10.5194/acp-6-5193-2006, 2006.

Yu, F. Q. and Turco, R. P.: Ultrafine aerosol formation via ion-mediated nucleation, Geophys. Res. Lett., 27, 883–886, https://doi.org/10.1029/1999gl011151, 2000.

Yu, F. Q. and Turco, R. P.: From molecular clusters to nanoparticles: Role of ambient ionization in tropospheric aerosol formation, J. Geophys. Res.-Atmos., 106, 4797–4814, https://doi.org/10.1029/2000jd900539, 2001.

Yu, T., Zhao, D., Song, X., and Zhu, T.: NO_2-initiated multiphase oxidation of SO_2 by O_2 on $CaCO_3$ particles, Atmos. Chem. Phys., 18, 6679–6689, https://doi.org/10.5194/acp-18-6679-2018, 2018.

Zhang, H., Chen, S., Zhong, J., Zhang, S., Zhang, Y., Zhang, X., Li, Z., and Zeng, X. C.: Formation of aqueous-phase sulfate during the haze period in China: Kinetics and atmospheric implications, Atmos. Environ., 177, 93–99, https://doi.org/10.1016/j.atmosenv.2018.01.017, 2018.

Zhao, D., Song, X., Zhu, T., Zhang, Z., Liu, Y., and Shang, J.: Multiphase oxidation of SO_2 by NO_2 on $CaCO_3$ particles, Atmos. Chem. Phys., 18, 2481–2493, https://doi.org/10.5194/acp-18-2481-2018, 2018.

Zhao, Y. and Truhlar, D. G.: The M06 suite of density functionals for main group thermochemistry, thermochemical kinetics, noncovalent interactions, excited states, and transition elements: two new functionals and systematic testing of four M06-class functionals and 12 other functionals, Theor. Chem. Account., 120, 215–241, https://doi.org/10.1007/s00214-007-0310-x, 2008.